Structures of the extracellular domain of the type I tumor necrosis factor receptor

James H Naismith[1]*, Tracey Q Devine[2], Tadahiko Kohno[3] and Stephen R Sprang[2,4]

Background: Tumor necrosis factor (TNF) is a powerful cytokine that is involved in immune and pro-inflammatory responses. Two TNF receptors that belong to the cysteine-rich low affinity nerve growth factor receptor family (TNF-R1 and TNF-R2) are the sole mediators of TNF signalling. Signalling is thought to occur when a trimer of TNF binds to the extracellular domains of two or three receptor molecules, which permits aggregation and activation of the cytoplasmic domains. The complex is then internalized within an endocytic vesicle, whereupon it dissociates at low pH. Structure of the soluble extracellular domain of the receptor (sTNF-R1) both in the unliganded and TNF-bound state have previously been determined. In both instances, the fourth subdomain of the receptor was found to be partly disordered. In the unliganded state at pH 7.5, the extracellular domain forms two distinct types of dimer, parallel and antiparallel; the antiparallel dimer occludes the TNF-binding.

Results: We have determined the structure of sTNF-R1 in two crystal forms in high salt at pH 3.7. The orthorhombic crystals diffract to 1.85 Å and the entire polypeptide is well ordered. In contrast, the C-terminal 32 residues are disordered in the hexagonal crystals. In the orthorhombic form, these residues exhibit a topology and disulphide connectivity that differs from the other three cysteine-rich domains in the molecule. In both forms, the interface is considerably more extensive than that used in complex formation with LTα. This 'low pH' dimer is different from both of the dimers observed in crystals grown at pH 7.5.

Conclusions: The occurrence of the antiparallel dimers in both low pH crystal forms suggest that they are not an artefact of crystal packing. Such dimers may form in the low pH environment of the endosome. Because the dimer contact surface occludes the TNF-binding site, formation of this dimer would dissociate the TNF–receptor complex within the endosome. Three of the four cysteine-rich domains of TNF-R1 are constructed from two distinct structural modules, termed A1 and B2. The fourth subdomain comprises an A1 module followed by an unusual C2 module. Although the orientation of these modules with respect to each other is sensitive to crystal packing, ligand binding, pH and ionic strength, the modules are structurally well conserved between and within the known sTNF-R1 structures.

Addresses: [1]Centre for Biomolecular Sciences, Purdie Building, The University, St. Andrews, KY16 9ST, Scotland, UK, [2]Howard Hughes Medical Institute, University of Texas Southwestern Medical Center, 5323 Harry Hines Blvd, Dallas, Texas TX75235-9050, USA, [3]Amgen Boulder Inc, 3200 Walnut St. Boulder, Colorado 80301, USA and [4]Department of Biochemistry, University of Texas Southwestern Medical Center, 5323 Harry Hines Blvd, Dallas, Texas TX75235-9050, USA.

*Corresponding author.
E-mail: naismith@st-andrews.ac.uk

Key words: crystal structures, molecular replacement, receptor, signalling, TNF

Received: 8 July 1996
Revisions requested: 27 July 1996
Revisions received: 20 August 1996
Accepted: 6 September 1996

Structure 15 November 1996, 4:1251–1262

Introduction

Tumor necrosis factor α (TNFα) and the closely related protein lymphotoxin (LTα/TNFβ) are now recognized as two of the most pleiotropic cytokines, signalling a large number of cellular processes, including cytotoxicity, apoptosis, antiviral activity and immunoregulatory activity [1]. The effects of TNF (denotes both cytokines) are signalled through two receptors: type I (55 kDa) and type II (75 kDa) [2–4]. The receptors belong to the cysteine-rich low affinity nerve growth factor receptor superfamily (NGF-R) which includes FAS, CD40, OX40, CD27 receptor and several viral proteins [5]. Across the family there is little primary sequence similarity among the extracellular domains, with the exception of the pattern of cysteines, and none at all within the intracellular domain. The receptors are structurally distinct from the cysteine knot class of proteins such as human chorionic gonadotropin (HCG) [6]. The X-ray structures of sTNF-R1 (the soluble extracellular domain of TNF-R1), both unliganded [7] and its complex with LTα [8], shows the receptor to be an elongated molecule, with a ladder-like progression of disulfide bonds along the long axis of the molecule. A linear combination of four subdomains was identified in the structure. The C terminus of the fourth subdomain is disordered in both structures and its primary sequence is inconsistent with the subdomain structure of the other three.

Figure 1

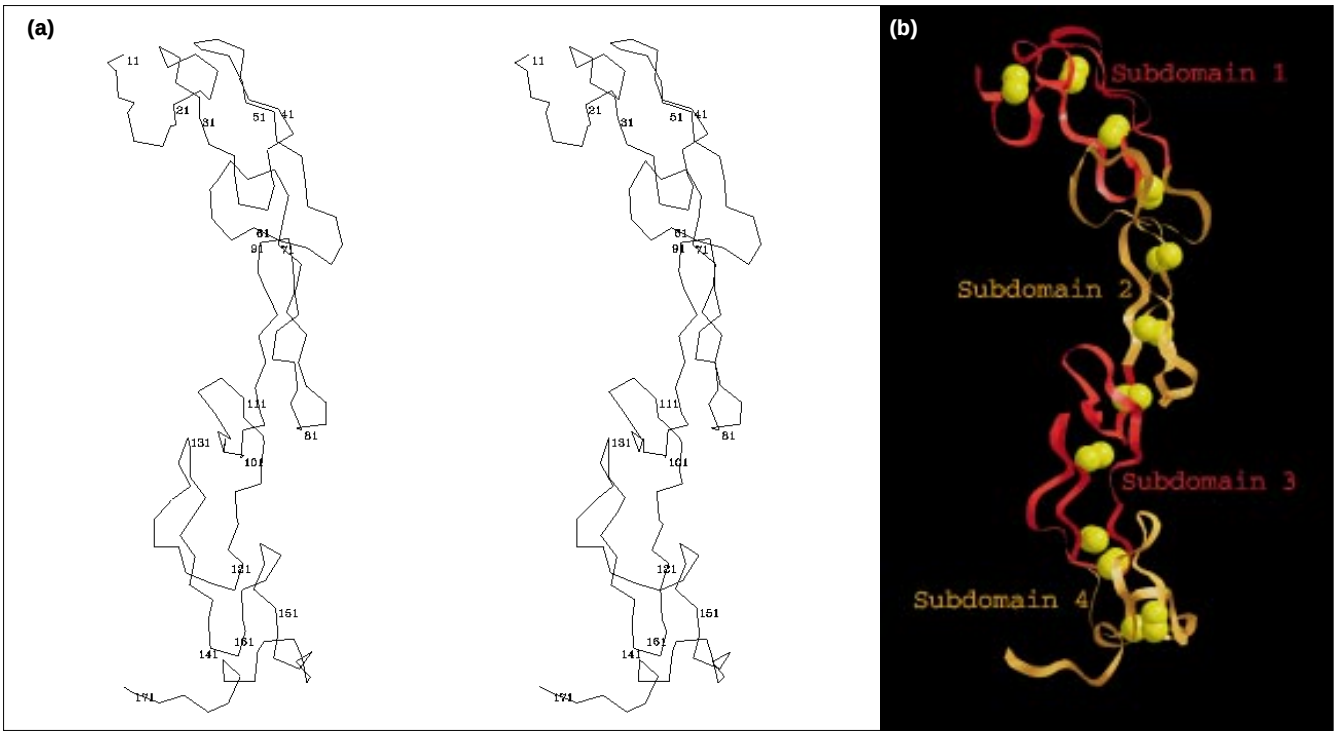

The complete structure of the monomer of sTNF-R1. (a) A stereo diagram of the numbered Cα trace of the sTNF-R1 molecule found at pH 3.7. (b) A ribbon representation of the structure with disulphide bonds shown as yellow spheres, prepared with RASTER3D [31]. Subdomains one and three are in red and subdomains two and four in orange.

Signal transduction occurs when TNF binds to the extracellular domains of two or three receptor molecules. This event promotes aggregation [9,10] of the intracellular domains, which in turn stimulates their interaction with a variety of other signalling molecules [11,12]. After signalling, the complex is internalized, and dissociates in the low-pH environment of the endosome [13]. The extracellular domain of the receptor is found as a soluble protein (sTNF-R1) in serum and may act to downregulate TNF signalling [14]. In the 2.85 Å crystal structure of LTα complexed to sTNF-R1 [8], three sTNF-R1 molecules are bound parallel to the LTα trimer axis. One sTNF-R1 molecule is bound at each of the three LTα–LTα interfaces. Interactions with LTα are confined to two clusters, essentially the C-terminal half of the second subdomain (residues 56–74) and much of the third subdomain (residues 77–81 and 107–114). The receptor extracellular domains do not contact each other in the complex.

The X-ray structure of unliganded sTNF-R1, crystallized from 2-methylpentan-2,4-diol (MPD) at pH 7.5 [7], raised the possibility that TNF release induces quaternary structural changes in the extracellular domain that could regulate the activity of the receptor. This structure showed that sTNF-R1 in the absence of TNF forms two distinct types of dimer one of which occludes the TNF- binding site [7]. A regulatory function for the ligand- binding domain is suggested by the aggregation and signalling activity shown by intracellular domains expressed in the cytosol in the absence of TNF [15]. In contrast, intact receptors are tightly regulated and silent in the absence of TNF. One interpretation of these results is that, in some way, the extracellular domains prevent 'false' signalling in the absence of TNF.

We suggested that dimerization of the extracellular domain could prevent signalling. We observed that one of the dimers, in which the extracellular domains are arranged in a parallel fashion, did not occlude the TNF-binding site. Such dimers could promote the formation of large cell surface aggregates that could play a role in complex internalization or may concentrate the signal within the cell. However, such aggregates were not observed in the crystalline LTα–sTNF-R1 complex [8].

We report two new structures of unliganded sTNF-R1, obtained at high ionic strength and pH 3.7. Both crystal forms diffract X-rays to d spacings less than 1.9 Å. In one form, the entire polypeptide chain (corresponding to residues 11–172 of full-length human TNF-R1) is ordered.

Figure 2

A disulphide connectivity diagram of (a) the third and (b) fourth subdomains. The disulphide connectivity is clearly different in the fourth subdomain.

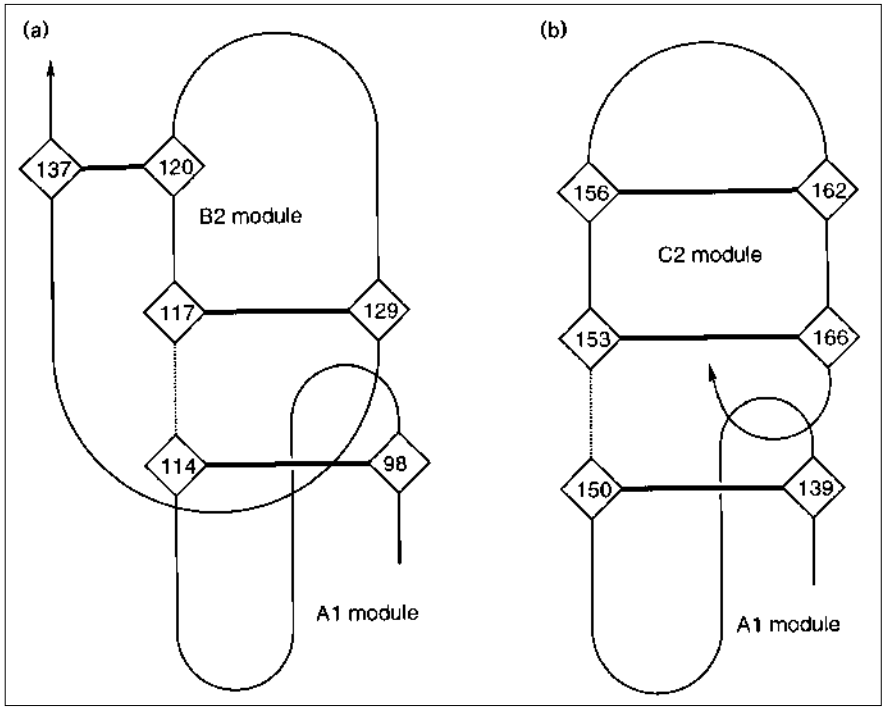

The C terminus of the fourth subdomain of sTNF-R1 has a different disulfide connectivity from that previously proposed [8] and a fold that is different from the C termini of the other three subdomains. At low pH the receptor is found as a dimer with extensive interactions between monomers, which occludes the TNF interaction surface. We suggest that this dimer may form during endocytosis, disrupting the TNF–TNF-R1 complex and allowing recycling of the receptor [16]. Consistent with an observation by Bazan [5], we find that each subdomain comprises two distinct types of structural modules. The modules, rather than the subdomains, are structurally conserved within the sTNF-R1 molecule.

Results and discussion

The monomer and the low pH dimer

From a concentrated solution of magnesium sulphate buffered at pH 3.7, crystals of sTNF-R1 appear simultaneously in hexagonal and orthorhombic space groups. The sTNF-R1 monomer (Fig. 1) found in the orthorhombic space group is highly elongated, with a solvent accessible surface area [17] of approximately 12000 Å^2 (0.48:0.52, apolar:polar) and an accessible surface to volume ratio of 0.72 Å^{-1}, seven times greater than for a sphere of equivalent volume. The monomer has no hydrophobic core but buries over 90% of the solvent-accessible area of the sulphur atoms in the disulphide bonds. The overall fold of the protein has been described [7,8]. The C terminus of the fourth subdomain (153–172), which was disordered in structures previously reported [7,8], is ordered in the orthorhombic crystals, but not in the hexagonal form. The disulphide pattern Cys3–Cys6 and Cys4–Cys5, is also different from the other subdomains (Fig. 2) which leads to a structure with a topology different from that observed in the other three subdomains (Figs 1,2). With the crystal structures described here, the structure of sTNF-R1 has been observed in six distinct packing environments. Within

Table 1

Interactions that constitute the dimers and LTα complex of sTNF-R1.

Interaction	pH 3.7 dimer	pH 7.5 antiparallel dimer	pH 7.5 parallel dimer	LTα complex
Hydrogen bonds*	12	11	11	14
van der Waals†	112	106	149	115
Ion pairs‡	1	2	1	4
Bridging waters	15	5	10	1
Contact surface§				
polar(Å^2)	1402	878	1064	1014
apolar(Å^2)	1480	1597	1079	1154
total(Å^2)	2882	1475	2143	2168
Complementarity#	0.65	0.70	0.67	0.66

*Contacts closer than 3.3 Å with appropriate stereochemistry; †contacts closer than 4.0 Å; ‡contacts closer than 3.3 Å involving two oppositely charged groups (at pH 3.7 we do not expect these to be charged interactions); §defined using a 1.4 Å probe [17]; #calculated by the method of Lawrence and Coleman [33].

Table 2

Non-bonded contacts between antiparallel dimers in orthorhombic (pH 3.7) crystals of sTNF-R1.

Polar contacts*					van der Waals
Residue A	Atom A	Residue B	Atom B	Distance (Å)	(≤4.0 Å)†
D12	–	–	–	–	N155
V14	–	–	–	–	R146, V151, L160(3)
C15	O	R146	Nη1	3.2	R146(2), L160(2)
P16	–	–	–	–	S159(2), L160, E161(2)
Q17	N	E161	Oε2	3.3	–
I21	–	–	–	–	E147(2)
F60	–	–	–	–	L111
H69	–	–	–	–	E79(4)
L71	–	–	–	–	R77, M80(2), L111
S72	O	R77	Nη1	3.2	R77(3)
	O	R77	Nη2	3.1	–
S74	–	–	–	–	R77
R77	Nη1	S72	O	3.1	L71(2), S72(3), D93
	Nη2	S72	O	3.2	–
	Nη2	S74	Oγ	3.3	–
E79	–	–	–	–	L67, L71
D93	–	–	–	–	L111
R104	Nη1	E109	Oε2	3.0	E109(2)
Y106	Oη	E109	Oε1	2.8	E109(4)
W107					S63(8)
N110	Oδ1	N110	Nδ2	2.7	N110(6)
L111	–	–	–	–	F60
F144	–	–	–	–	V14(2)
R146	Nη1	C15	O	3.0	V14(3), C15(4), P16, Q17(2)
E147	Oε1	C15	N	2.9	M11(2), V14(5), C15(4)
V151	–	–	–	–	M11(2), V14
N155	–	–	–	–	D12(14)
S159	–	–	–	–	P16(2)
L160	–	–	–	–	V14
E161	Oε1	Q17	N	2.8	P16(6), Q17(3)

*Hydrogen bond and ion pairs between atoms from monomer A and atoms from monomer B (cut-off is 3.3 Å). Residues are identified by the one letter code and sequence number. †For each residue in monomer A, van der Waals partners in monomer B are listed. The number in parentheses indicates the number of atoms in that residue within 4.0 Å of the corresponding residue in monomer A.

this group, the conformation of the C-terminal subdomain ranges from completely disordered to fully ordered.

In both crystal forms, the prominent structural unit is a dimer of sTNF-R1 molecules (Fig. 3). However, the packing arrangements by which the dimer is organized within the hexagonal and orthorhombic cells differ. The conservation of this dimer in the context of two different crystal-packing arrangements suggests that dimer formation is driven by solvent environment and pH rather than crystal-packing forces. The sTNF-R1 dimer found in the orthorhombic and hexagonal crystal forms is different from both of the dimers we previously observed in the tetragonal crystal form grown from MPD at pH 7.5 (Fig. 4) [7]. Although these differences in the dimer association between the tetragonal and orthorhombic/hexagonal forms may be attributed to either pH and/or the solvent conditions, we refer to the dimers either as 'high pH' (tetragonal) and 'low pH' (orthorhombic, hexagonal). Like one of the two high pH dimeric species, the low pH dimer is formed by an antiparallel (head-to-tail) arrangement of the monomers. Unlike the antiparallel high pH dimer (Fig. 4b), the two monomers completely overlap, such that the length of the dimer is 90 Å, almost identical to that of a single monomer. There appears to be no obvious explanation for why one dimer is favoured under different solvent conditions. The low pH dimer remains extremely non-globular with an accessible surface to volume ratio of 0.64 $Å^{-1}$ (nearly six times greater than for a sphere of equivalent volume). In the orthorhombic form, a noncrystallographic twofold axis relates the monomers. The N terminus of monomer 2 interacts extensively with the C terminus of monomer 1, presumably ordering the two termini. However, the opposite pair of termini do not form such close contacts with each other, leading to disorder in residues 11 and 12 in monomer 1 and residues 168–171 in monomer 2. In the hexagonal crystal form an essentially identical dimer is generated by a crystallographic twofold axis. However, the C-terminal 32 residues are disordered in this structure.

Figure 3

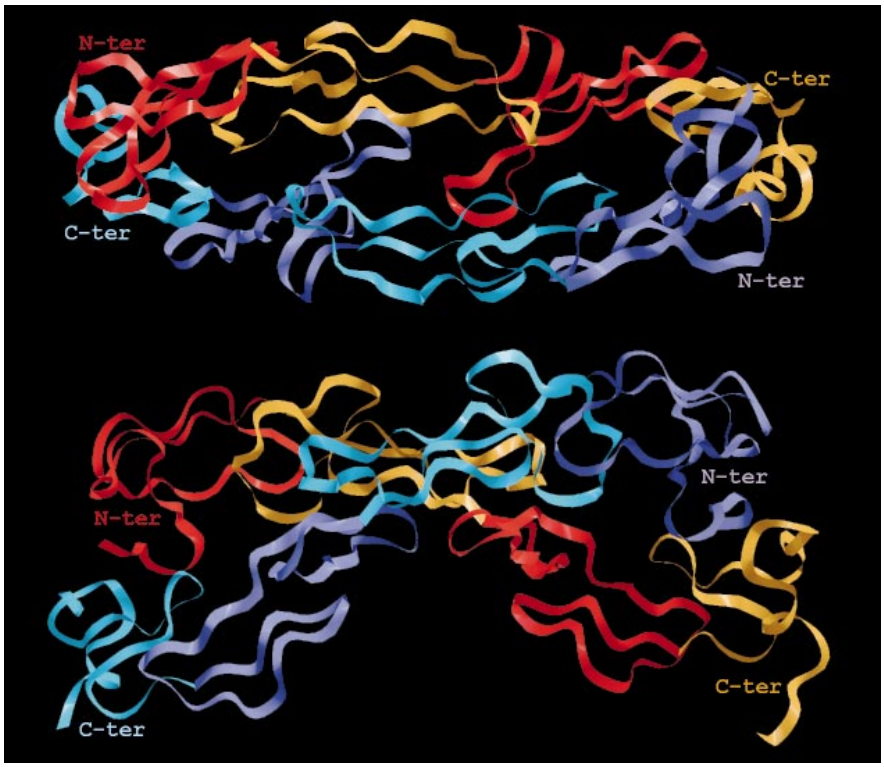

Two orthogonal views of the low pH dimer that is the asymmetric unit of the $P2_12_12_1$ crystal form. Careful examination of the figure shows that the interaction between subdomain one and subdomain four is closer at one end of the dimer than the other. (Figure prepared using RASTER3D [31].) The color scheme for one monomer is the same as in Figure 1. The other monomer is colored dark blue (subdomains one and three) and bright blue (subdomains two and four).

The low pH dimer is held together by extensive hydrophobic and hydrophilic interactions that bury 1480 Å^2 of hydrophobic accessible surface and 1400 Å^2 of hydrophilic accessible surface These interactions, which are detailed in Tables 1 and 2, occur along the entire length of the dimer. Two cavities (related by the twofold axis) are formed at the dimer interface with residues 17, 18, 32 and 67 from one monomer and residues 113, 115, 134, 148 from the other. The cavity has an approximate diameter of 10 Å, and is partially filled with ordered water molecules. In addition, the twofold axis of the dimer passes through a narrow twisted solvent channel with a diameter no greater than 3.0 Å. Unlike the recombinant protein described here, the extracellular domain of the native receptor is glycosylated at Asn17, 96 and 124. However, as these sites are not located at the dimer interface they would be expected not to interfere with dimerization.

The surface area buried by the low pH dimer is comparable with that observed in other multimeric proteins [18] and far exceeds that commonly seen for antibody–antigen interactions [19]. Perhaps the most interesting observation is that the low pH dimer buries almost 50% more surface area than the LTα–sTNF-R1 complex [8]. Residues 14–17, 21, 60, 69–72, 77–79, 104–107, 110–114, 144, 146–147, 151–155, 160–161 are involved in or are buried by formation of the low pH dimer (Table 2), encompassing virtually all the residues involved in LTα– recognition [8]. This dimer would therefore be incapable of binding TNF in the manner observed in crystals of the LTα–sTNF-R1 complex [8]. It is notable that the LTα complex is stabilized by four ion pairs; we would expect these to be much weaker at low pH. The low pH dimer bears a further superficial resemblance to the high pH antiparallel dimer: both bury the TNF interaction surface. However, although some residues (His69, Leu71, Ser72, Arg77, Glu79 and Asp93) are present at both interfaces, the dimers are formed by completely different sets of residue–residue contacts (Tables 2 and 3). The parallel dimer found at high pH which does not occlude the TNF interaction surface is held together by an almost completely different subset of residues and contacts than either of the antiparallel dimers (Tables 2, 3 and 4).

As yet no direct evidence exists to support a dimeric receptor species in solution. Nevertheless, in the relevant biological context, TNF-R1 dimers are proposed to form on the two-dimensional surface of the plasma membrane where the entropy penalty for dimerization would be significantly less than for dimer formation in solution [20].

Modular structure of sTNF-R1

The extracellular domains of TNF-R1 and its homologues have been characterized as multiple repeats of an

Table 3

Non-bonded contacts between antiparallel dimers in tetragonal (pH 7.5) crystals of sTNF-R1.

Polar contacts*					van der Waals
Residue A	Atom A	Residue B	Atom B	Distance (Å)	(4.0 Å)†
Q24	–	–	–	–	S108(2)
Y40	O	R77	Nη2	2.7	C76, R77(18), E79(5)
N41	–	–	–	–	L111
R53	Nη2	E79	Oε2	2.9	E79(3)
S59	–	–	–	–	S72
F60	–	–	–	–	H69(3)
H69	Nδ1	S72	O	2.8	F60(3), L71(2), S72(6),S74(2), D83
C70	N	S72	Oγ	2.8	C70, L(2), S72(8)
	O	S72	N	2.9	–
L71	–	–	–	–	H69(3), C70(2)
S72	N	C70	O	2.9	S59, H69(6),C70(7)
	Oγ	C70	N	2.9	–
	O	H69	Nδ1	2.7	–
S74	–	–	–	–	H69(2)
K75	Nζ	E56	Oε1	2.9	Y38, E56
C76	–	–	–	–	Y40
R77	Nη1	Y40	O	3.0	Y40(8), N41(7)
Nη2	Y40	O	2.6	–	–
K78	–	–	–	–	Y40
E79	Oε1	Y40	Oη	2.7	Y40(7)
	Oε2	N41	Nδ2	3.2	–
D93	–	–	–	–	H69

*Hydrogen bond and ion pairs between atoms from residues in monomer A with atoms from residues in monomer B (cut-off is 3.3 Å). Residues are identified by one letter code and sequence number. †For each residue in monomer A, van der Waals partners in monomer B are listed. The number in parentheses indicates the number of atoms in that residue within 4.0 Å of the corresponding residue in monomer A.

approximately 40-residue subdomain. The subdomain has the sequence Cys1–$x_{10\text{-}15}$–Cys2–x_2–Cys3 –x_2–Cys4–$x_{8\text{–}11}$–Cys5–$x_{7\text{–}8}$–Cys6, where $x_{n\text{–}m}$ denotes n to m intervening amino acids. The subdomain is characterized by three disulphides: Cys1–Cys2, Cys3–Cys5 and Cys4–Cys6. This structural unit is exemplified by subdomains two (55–96) and three (98–137) of sTNF-R1 and has been described in detail [7,8]. However, subdomain one (15–52), has no intervening residues between Cys2 and Cys3. As a result, the orientation of the N-terminal S-shaped loop relative to the C-terminal S-shaped loop is quite different when compared with subdomains two and three (Figs 1,2). Subdomain four (139–166) is yet more divergent, as discussed above.

In accordance with Bazan [5], we now suggest that the extracellular domain of TNF-R1 is built up of three distinct modules, which we term A1, B2 and C2, rather than the 40-residue subdomain favoured in earlier reports [7,8]. A and B modules may contain either one or two disulfide bonds, thus giving rise to the designation A1, B2 etc. The A1 module is the N-terminal S-shaped loop found in all four subdomains. The B2 module is the C-terminal S-shaped loop found in subdomains one, two and three. The C2 module corresponds to the C terminus of the fourth subdomain, which is disordered in all but the orthorhombic crystals. Subdomains one, two and three are each a linear combination of an A1 and a B2 module. Subdomain four is a linear combination of an A1 and a C2 module. Figure 2 shows how a subdomain is decomposed into its constituent modules and Figure 5 shows the structure of the A1 and B2 modules. The modules are connected to each other by a varying number of intervening acids (0, 1 and 2). The modular composition of sTNF-R1 is shown in Figure 6.

The four A1 modules have the sequence Cys1–x_2–Gly–x_1–Tyr(Phe)–$x^a{}_1$–$x^b{}_{4\text{–}9}$–Cys2: we use superscripts to identify particular residues or regions within the structure. Each module has a structurally conserved core of eight amino acids (Cys1–x_2–Gly–x_1–Tyr–$x^a{}_1$ and Cys2) whose Cα atoms superimpose with an average root mean square (rms) deviation of 0.4 Å (Fig. 5a). This core includes the conserved aromatic residue highlighted by Banner *et al.* [8]. Structural variability is seen at the $x^b{}_{4\text{–}9}$ loop (at the bottom of Fig. 5a). Each A1 module has a different sequence and number of amino acids in this loop. The B2 modules at residues 73–96 and 117–137 have sequence Cys3–x_2–Cys4–$x^c{}_{3/6}$–$x^d{}_5$–Cys5–$x^e{}_4$–Asp–Thr–x–Cys6 where n/m denotes n or m intervening

Figure 4

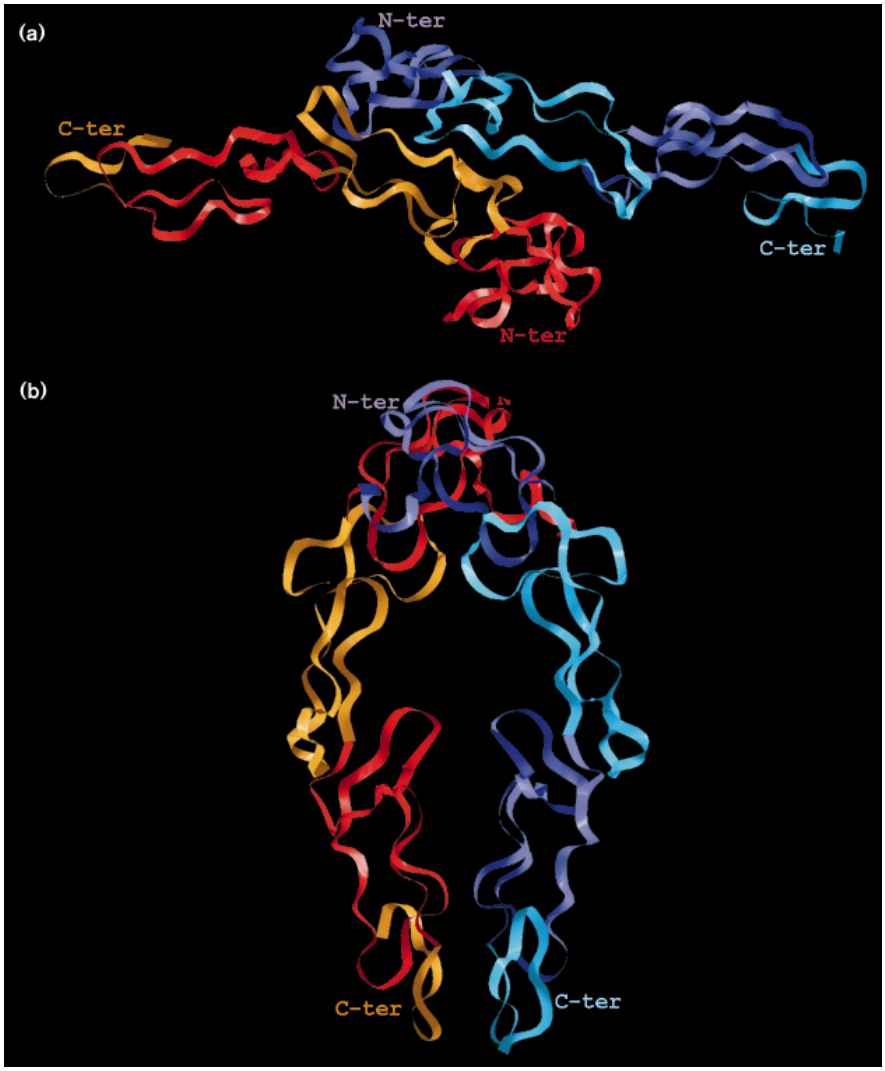

(a) The parallel dimer found at pH 7.5; this dimer does not occlude the TNF-binding site. (b) The antiparallel dimer found at pH 7.5 occludes the TNF-binding site. The color scheme is as in Figure 3. (Figure prepared using RASTER3D [31].)

residues. This gives 18 superimposable amino acids with a Cα rms deviation of 0.7 Å. The loop $x^{c}_{3/6}$ (top of Fig. 5b) is different in both sequence and in the number of amino acids; it was therefore excluded from the superposition calculation. The B2 module in subdomain one (residues 30–52) again has a different loop composition four residues) and structure at x^{c}. However, it also differs in that it has five rather than four residues at x^{e}. This results in only 14 superimposable amino acids with an average rms deviation of 0.8 Å for Cα atoms. The conserved core of amino acids includes the Asp–Thr–x–Cys6 motif highlighted previously [8].

It is notable that in both modules, structural divergence is associated with differing numbers of residues in a loop and that sequence divergence occurs in structurally conserved loops. For instance the glycine in the A1 module is replaced by asparagine in subdomain three. We therefore suggest, that it is the number, rather than the type, of residues that determines the structure of variable loop regions in the A1 and B2 modules. We have extended our analysis to the entire TNF-R superfamily (JHN and SRS, unpublished data) and have found that the vast majority of TNF-R1 homologues can be described as combinations of A and B modules.

Segmental flexibility: structural differences on pH change and LTα binding

The low pH form in combination with other structures of sTNF-R1 allows us to describe the changes in receptor conformation that occur in response to environment. Table 5 summarizes the results of the superpositions of the six sTNF-R1 structures. When the monomer is considered as a single unit, the rms deviations in Cα positions range from 1.1 to 2.8 Å. For monomers related by noncrystallographic symmetry (ncs), the rms deviation is 1.4 Å. Splitting the

Table 4

Non-bonded contacts between parallel dimers in tetragonal (pH 7.5) crystals of sTNF-R1.

Polar contacts*					van der Waals
Residue A	Atom A	Residue B	Atom B	Distance (Å)	(≤4.0Å)†
M11	E54				
Q17	Nε2	K35	O	3.3	T37(4), K35, G36(3), E54, V90(2), D91
G18					H34(5)
K19	Nζ	D49	Oδ2	3.1	D49(2)
T31	Oγ1	D49	Oδ1	2.7	H34(2), D49(3)
K32	O	H34	Nε2	2.8	H34(8)
C33					H34(2)
H34	Nε2	K32	O	2.8	G18(2), T31(2), K32(8), C33(2), H34(8), E64(3)
K35	O	Q17	Nε2	3.1	Q17(2), E64(3)
G36					Q17(4)
T37					Q17(3)
G47	O	D49	N	2.9	Q48(3), D49(4)
Q48	Nε2	Q48	Oε1	2.9	G47(4), D48(4), Q49(7)
D49	N	G47	O	2.9	K19(2), T31(4), G47(4), Q48(3),
	Oδ2	T31	Oγ1	2.6	D49(2)
E54					Q17
E64					H34(4), K35(2)
V90					Q17(2)
D91					Q17
H126					V136(2), L145
L127					Q133, V136
Q130					Q133(2)
Q133	Oε1	Q133	Nε2	2.9	L127, Q130(3), Q133(6)
	Nε2	Q133	Oε1	2.9	
V136					H126(2), L127, V136
C137					H126(2)
T138					L145
L145					H126(5), T138

*Hydrogen bond and ion pairs between atoms from residues in monomer A with atoms from residues in monomer B (cut-off is 3.3 Å). Residues are identified by the one letter code and sequence number.

†For each residue in monomer A, van der Waals partners in monomer B are listed. The number in parentheses indicates the number of atoms in that residue within 4.0 Å of the corresponding residue in monomer A.

monomers into the four subdomains reduces these values and splitting the structures into modules reduces them to ≤0.5 Å (i.e. more typical values for structural superposition). Thus it is the modules which are structurally conserved among the structures of sTNF-R1 rather than the subdomains. The high rms deviations for the monomer and subdomain superpositions are due to structural flexibility in the connections between modules. These connections are equally flexible whether they are within or between subdomains. For example, the ncs superposition of residues 30–70 (B2–A1 module combination with connection between subdomains) is 0.4 Å, approximately the same as residues 55–96 (A1–B2 module combination with connection within a subdomain). Splitting subdomain one into two modules yields a less dramatic drop in rms deviation, a consequence of the lack of intervening residues between the modules and hence decreased flexibility. The most pronounced flexibility is seen at Gly97, the connection between the second and third subdomains (Fig. 7). It is the segmental rigid-body movements of modules that underlie deviations from ncs in sTNF-R1.

Segmental flexibility allows sTNF-R1 to adapt its structure to changes in solvent conditions and LTα binding. These adaptations are most dramatically illustrated by superimposing all structures of sTNF-R1, but using only

Table 5

Root mean square deviations (Å) in Cα superpositions.

Reference	Target molecules for superposition			
orthorhombic*	Orthorhombic†	Hexagonal	Tetragonal	LTα complex
Monomer	1.4	1.1	2.9	1.8
Subdomains	0.4	0.5	0.8	0.7
Modules	0.2	0.4	0.5	0.5

*Monomer A of the orthorhombic crystal form; †monomer B of the orthorhombic crystal form.

Figure 5

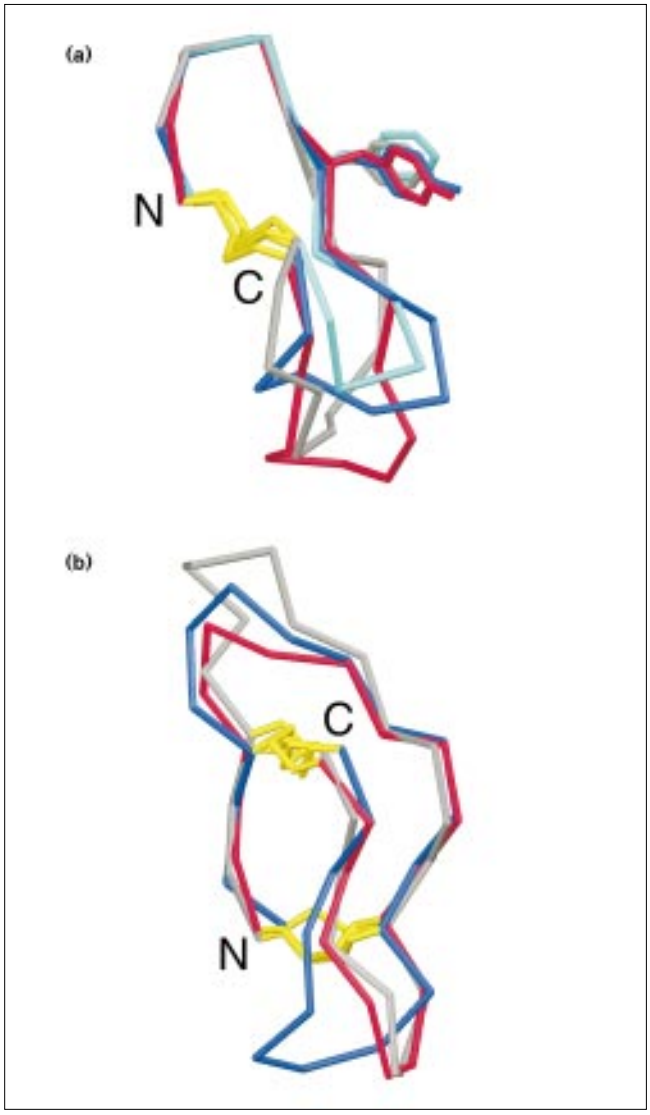

The modules which are structurally conserved within sTNF-R1. (a) An overlay of the four type A modules found in sTNF-R1: residues 15–29 (dark blue); residues 55–70 (grey); residues 98–114 (red); and residues 139–150 (light blue). The side chains of the conserved aromatic residues are shown, the cysteine residues are shown in yellow. (b) An overlay of the three type B modules found in sTNF-R1: residues 30–52 (blue); residues 73–96 (grey), and residues 117–137 (red). Cysteine residues are shown in yellow. Figure prepared using SETOR [32].

Figure 6

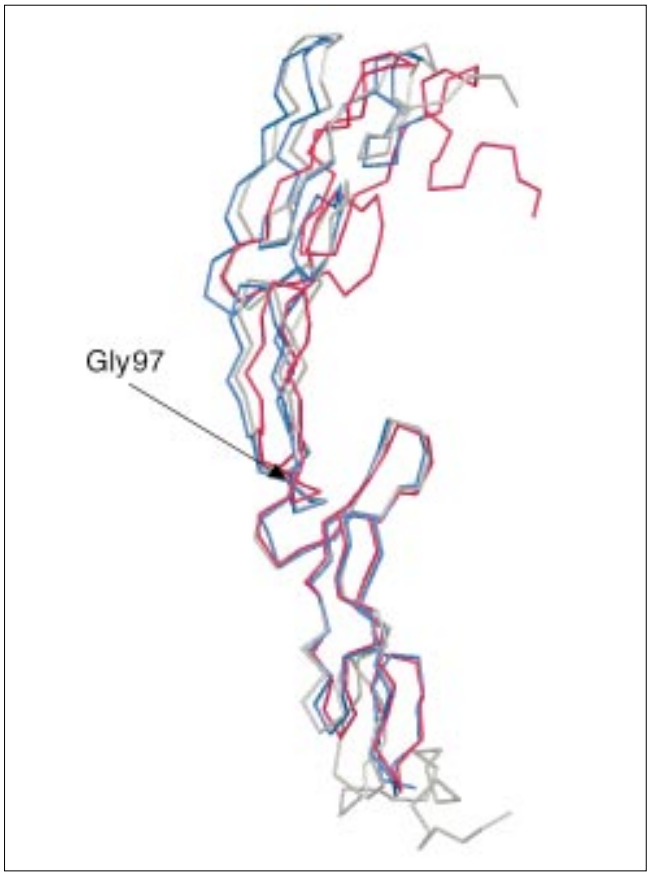

Superposition of sTNF-R1 monomers from the orthorhombic (low pH) crystal form (grey), tetragonal (pH 7.5) crystal form (red) and LTα complex (blue). The superpositions were calculated using only the Cα atoms of subdomain three. The segmental flexibility of the monomer is clear, with dramatic shifts in the N-terminal subdomains. The fourth subdomain of the orthorhombic crystal form is clearly positioned differently from the other two. (Figure prepared using SETOR [32].)

residues in subdomain three to calculate the superposition vector (Fig. 7). This partially mimics the biological environment where the C terminus is anchored to the membrane. This superposition results in a difference of over 15 Å in the position of N terminus between the high [7] and low pH forms of the receptor. The LTα-bound form of sTNF-R1 [8] lies between these extremes. As a result, the low pH monomer is less curved with a distance between the first and tenth disulphide of 66 Å compared with 62 Å at pH 7.5 and 64 Å in the LTα-complex form. The fourth subdomain adopts a different orientation relative to third subdomain in the low pH form when compared with the other structures. This shift in position is over 4.0 Å and is clearly visible in Figure 7. We interpret the movement of the fourth subdomain as being a consequence of its participation in dimer contacts and the hydrogen bonds that it forms to the third subdomain; Asn148 to Asn116 and Asn148 to Ser118. Both this dimer and these additional hydrogen bonds are unique to the low pH crystals. In the orthorhombic structure the ninth disulphide (Cys129–Cys137) adopts unusual $\chi 1$ values of 180°/180°, in contrast to the pH 7.5 and LTα complex structures where the corresponding values are 60°/60°. The conformation of the ninth disulphide in the hexagonal form is ambiguous. It seems likely that this change in

Table 6

Crystal parameters, data collection and refinement statistics.

	$P2_12_12_1$	$P6_122$
Unique reflections	37300	13334
Completeness of data		
entire resolution range $I > 0\sigma I$ ($> 3\sigma I$)	11.0–1.85 Å 97% (91%)	42.0–1.87 Å 97% (88%)
highest resolution shell $I > 0\sigma I$ ($> 3\sigma I$)	1.93–1.85 Å 77% (64%)	1.95–1.87 Å 91% (68%)
$R_{merge}(I)$ (%)*	5.1	5.5
Average data redundancy	5	6
Refinement		
Resolution range (Å)	8–1.85	42–1.87
R free (%)†	24.3	27.8
R factor (%)	20.5	23.9
Bond rms deviation (Å)‡	0.009	0.009
Angle rms deviation (Å)‡	1.686	1.790
Ramachandran core/addtnl (%)§	90.2/9.8	85.0/12.0
Protein mean B ($Å^2$)	18	35
Solvent mean B ($Å^2$)	30	43
B-factor bond rms deviation (Å)#	2.0	3.4
Protein atoms	3080	1255
Solvent atoms	403	120

*$R_{merge(I)} = \Sigma_{hkl}\Sigma_i | I_i - I(hkl)| / \Sigma_{hkl}\Sigma_i I_i(hkl)$; †R free is calculated on 10% of data excluded from gradient calculation during refinement; ‡rms deviation from Engh and Huber ideal values [28]; §core and additionally allowed regions as defined by PROCHECK [29]. In $P6_122$, one residue is in the generously allowed region and two are in disallowed regions; all three residues are in poorly defined regions of electron density. #Rms deviations on B factors between bonded atoms, calculated with MOLEMAN (GJ Kleywegt, unpublished program); atoms with zero occupancy are excluded from all B factor calculations.

disulphide conformation is correlated with the movement of the fourth subdomain. We note that constructing a model of the parallel dimer form seen at pH 7.5 (Fig. 4a) with the complete monomer leads to interpenetration of subdomain four, strongly suggesting that the position of this subdomain is flexible. Comparing the two unliganded structures, shifts in local regions of the main chain (up to 1.0 Å) occur at regions that are involved in dimer or crystal contacts, particularly at Pro46, Ser74 and Val90. In the LTα complex, the main chain at Asn25 is shifted relative to both unliganded structures. However, this may reflect the fact that in the LTα complex structure, this residue was glycosylated. The orientation of side chains at Ser63, 72 and 108 change on LTα binding in order to make hydrogen bonds with the cytokine. A number of other differences in side-chain conformation are seen, but these are either found in flexible regions or differ between the various unliganded receptor structures.

Biological implications

Tumor necrosis factor (TNF) is responsible for dramatic changes in cellular metabolism. TNF exerts its affects through two receptors, TNF-R1 and TNF-R2. Both receptors belong to a superfamily that includes FAS, low affinity nerve growth factor (NGF) receptor and CD40. We report the crystal structure of the extracellular domain of the TNF-R1 receptor (sTNF-R1), crystallized at low pH and at high ionic strength; the receptor exists as a dimer in two crystal forms. The dimer is formed by an antiparallel association between the monomers at a dimerization interface that overlaps with the LTα-binding surface. The interface is considerably more extensive than that involved in complex formation with LTα. We do not claim that acidic conditions are specifically responsible for the formation of the sTNF-R1 dimers observed in the orthorhombic crystals. However, such dimers could form when TNF-bound receptors are internalized and enter the acidic compartment of the endosome. Dimer formation would displace bound TNF and could allow the receptors to be recycled. We have previously shown that sTNF-R1 crystallized at pH 7.5 from methylpentandiol forms both an antiparallel and a parallel dimer, which are distinct from the dimer described here. We suggested possible roles for 'high pH' dimers in signal regulation and receptor internalization. No direct evidence exists to support a dimeric receptor species in solution. Nevertheless, the entropy penalty for dimerization on the membrane would be significantly

Figure 7

15–29		30–52		55–70		73–96		98–114		117–137		139–150		153–166
A1	x_0	B2	x_2	A1	x_2	B2	x_1	A1	x_2	B2	x_1	A1	x_2	C2
subdomain one				subdomain two				subdomain three				subdomain four		

less than for dimer formation in dilute solution. Further studies of the aggregation properties of the receptor *in vivo* will be required to assess the true biological relevance of ligand-independent receptor aggregation.

Three of the four ~40 amino-acid subdomains that comprise the extracellular domain of TNF-R1 are composed of a linear combination of an A1 module and B2 module. The A1 module is the S-shaped double hairpin structure that forms the N-terminal half of the subdomain. The B2 module is a similar but distinct S-shaped structure that forms the C-terminal half of the subdomain. The fourth subdomain, which had been largely disordered in all previous studies, consists of an A1 module followed by an atypical C2 module. The C2 differs in topology and disulphide connectivity from both the A1 and B2 modules. Elsewhere, we demonstrate that all members of the TNF-R superfamily are combinations of modules. In sTNF-R1 it is the modules rather than the subdomains that are structurally conserved. The connections between the modules are flexible: consequently, sTNF-R1 exhibits segmental rigid-body movements in response to pH changes and LTα binding. Modules may correspond to functional as well as structural units. The compartmentalization of binding activity within small, discrete structural units has important implications both for the evolution of this family of receptors, and for the design of receptor antagonists.

Materials and methods

Crystallization and data collection

Recombinant sTNF-R1 was expressed and purified as previously described [21]. Although the protein used was refolded from inclusion bodies, kinetic and thermodynamic measurements indicate that it is identical to the protein found in serum and urine. Crystals in space group $P2_12_12_1$, with unit-cell parameters a = 78.8 Å, b = 83.1 Å, c = 67.9 Å were obtained at pH 3.7 with $MgSO_4$ as the precipitant, as described [21]. More recent batches of protein have produced a second crystal form under exactly the same conditions as used for the $P2_12_12_1$ form. This form occurs as hexagonal bipyramids in spacegroup $P6_122$ with unit-cell parameters a = b = 69.5 Å, c = 112.8 Å. The percentage of each form varies from 0–100% within any crystallization experiment, although $P2_12_12_1$ predominates. We have as yet found no systematic way of selecting one form over the other. We cannot identify any changes in the protein from one batch to the next and we have not modified our purification or crystallization protocols. All batches of the protein crystallize at pH 7.5 with MPD [21]. Although we think it is highly unlikely, we cannot exclude the possibility of the presence of folding isomers (at the C terminus).

Data to 1.85 Å for the $P2_12_12_1$ crystal form were collected from a single frozen crystal mounted in a nylon loop at Station PX9.2 at the Daresbury synchrotron, with a wavelength of 0.992 Å on a Mar image plate. The crystal was cryoprotected with 12% glycerol prior to data collection. The intensity data were processed and merged with DENZO and SCALEPACK [22]. Further data reduction was carried out with the CCP4 package [23]. Data reduction statistics are shown in Table 6. The first data set on the $P6_122$ form was recorded with a room temperature crystal using the Xuong-Hamlin area detector and a copper rotating anode source. The crystal was radiation sensitive and only a 60% complete 2.8 Å data set was recorded. A second data set on a cryoprotected (12% glycerol) $P6_122$ crysta was collected to 1.87 Å using an R-AXIS II with a copper rotating anode source. The intensity data were processed and merged with DENZO and SCALEPACK [22]. Data reduction statistics for the frozen $P6_122$ crystal are shown in Table 6.

Structure solution and refinement

The $P2_12_12_1$ crystal form had not proven tractable to isomorphous replacement. Molecular replacement using sTNF-R1 dimers or monomers or partial structures thereof from the $P4_12_12$ structure [7] and the LTα complex [8] failed to yield a solution. The room temperature data set on the $P6_122$ crystal form then came to hand. With a monomer in the asymmetric unit this crystal form was readily solvable with CCP4 AMORE [24] using a monomer from the $P4_12_12$ structure [7] as the search model. Despite the poor quality of the data this structure was refined to an R factor of 25%, and R free of 38%. The structure was ordered only from residues 15–137 and electron density was weak and noisy for residues 110–137. This partially refined partial structure was used as a model for a further molecular replacement attempt on the $P2_12_12_1$ structure. This search model produced a single weak solution with CCP4 AMORE, but only when normalised structure factors (Es) were employed. This single solution readily located the second monomer in a phased translation search. The two monomers were not related by any peak in the Patterson self-rotation map.

The $P2_12_12_1$ structure was refined using X-PLOR [25] and manual intervention was carried out using O [26]. Electron-density maps were calculated with data from 11–1.85 Å using SIGMAA-weighted coefficients [27]. The model was refined against 90% of the measured data between 8–1.85 Å using the Engh and Huber stereochemical dictionary [28]. The remaining 10% of measured data between 8 and 1.85 Å were excluded from all refinement calculations to monitor progress of refinement. No sigma cut-off was applied to the data. Weak noncrystallographic restraints were imposed on both positional and B-factor refinement, but regions of crystal contact were excluded. The initial model (R = 55%, R free = 54%) had to be extensively rebuilt, particularly residues 97–137. It was immediately obvious in the first F_o–F_c maps that a large C-terminal portion of the molecule was present. Residues 138–172 for one monomer and 138–168 for the other were built into density. Water molecules were included in batches provided they satisfied four criteria: they corresponded to a peak at $\geq 3.5\sigma$ (0.26e/Å^{-3}) in the F_o–F_c map; they formed potential hydrogen bonds with reasonable stereochemistry; they reappear in at least 1σ in subsequent $2F_o$–F_c maps (0.26e/Å^{-3}); and adding the batch of water yielded a reduction in R free. Once convergence was achieved, the model was then refined against all measured data from 8 to 1.85 Å for 20 cycles of Powell minimization. Statistics on the final model are shown in Table 6.

To confirm the difference in the conformation of disulphide nine between the orthorhombic and tetragonal structures, we calculated simulated-annealing SIGMAA omit maps for both structures. We also rebuilt each like the other and attempted to refine these models. However, difference electron density strongly suggested that the original conformers were correct in each case. We are convinced that this is a real difference in the structures.

The 1.87 Å data set on the $P6_122$ crystal was collected after the $P2_12_12_1$ structure had been fully refined. The hexagonal structure was redetermined using CCP4 AMORE with a monomer from the orthorhombic structure. The C-terminal 34 residues had to be removed from the search model to yield the correct solution. This structure was refined using data (no sigma cut-off) from 42–1.87 Å with the X-PLOR bulk solvent correction [25]. Statistics on the final model are shown in Table 6. The $P6_122$ structure is extremely disordered in some residues: only residues 14–120 and 127–135 are ordered. Residues 13, 121–127 and 135–139 were built into weak and ambiguous density on the basis of prior sTNF-R1 structures. Residues 11, 12 and 140–172 appear to be completely disordered, consistent with our observation that including this region in the search model gives an incorrect solution. We feel that

our failure to accurately model these disordered regions is responsible for the relatively high R free of 27.8%.

Protein stereochemistry was assessed with X-PLOR [25] and PROCHECK [29]. Programs from the Uppsala suite were used to measure differences in dihedral and side-chain angles between monomers. Superpositions and buried surface area calculations were carried out using the CCP4 package [23].

Accession numbers

The coordinates of the $P2_12_12_1$ dimer and the data set have been deposited with the Brookhaven Protein Data Bank [30] (entry codes 1EXT and R1EXTSF).

Acknowledgements

We thank Mike Eck, Barbara Brandhuber and Lynn Rodseth for early contributions to the project; Albert Berghuis, Sean McSweeny, Peter Lindley and Elizabeth Duke for help with data collection at Daresbury; Bryan Sutton for skilled assistance with figures. We are grateful to John Tesmer for his assistance in measuring and processing the high resolution $P6_122$ data set. We thank Werner Lesslauer and Dave Banner (Hoffmann La Roche) for prerelease of the LTα–sTNF-R1 complex coordinates. We thank the reviewers and editors for helpful comments. JHN acknowledges the Wellcome Trust (043586/Z/95/Z/RF/PK), the University of St. Andrews and the BBSRC (ref 49/B06675) for support, and the Daresbury Laboratory for data collection facilities.

References

1. Beutler, B. (1992). *The tumor necrosis factors: the molecules and their emerging roles in medicine*. Raven Press, New York, USA.
2. Smith, C.A., *et al*., & Goodwin, R.G. (1990). A receptor for tumor necrosis factor defines an unusual family of cellular and viral proteins. *Science* 248, 1019–1023.
3. Schall, T.J., *et al*., & Goeddel, D.V. (1990). Molecular cloning and expression of a receptor for human tumor necrosis factor. *Cell* 61, 361–370.
4. Loetscher, H., *et al*., & Lesslauer, W. (1990). Molecular cloning and expression of the human 55 kda tumor necrosis factor receptor. *Cell* 61, 351–359.
5. Bazan, J.F. (1993). Emerging families of cytokines and receptors. *Current Biology* 3, 603–606.
6. Lapthorn, A.J., *et al*., & Isaacs, N.W. (1994). Crystal structure of human chorionic gonadotropin. *Nature* 369, 455–461.
7. Naismith, J.H., Devine, T.Q., Brandhuber, B.J. & Sprang, S.R. (1995). Crystallographic evidence for dimerization of unliganded tumor necrosis factor receptor. *J. Biol. Chem*. 270, 13303–13307.
8. Banner, D.W., *et al*., & Lesslauer, W. (1993). Crystal structure of the soluble human 55 kda TNF receptor-human TNFβ complex: Implications for TNF receptor activation. *Cell* 73, 431–445.
9. Song, H.Y., Dunbar, J.D. & Donner, D.B. (1994). Aggregation of the intracellular domain of the type 1 tumor necrosis factor receptor defined by the two-hybrid system. *J. Biol. Chem*. 269, 22492–22495.
10. Grazioli, L., Casero, D., Restivo, A., Cozzi, E. & Marcucci, F. (1994). Tumor necrosis factor-driven formation of disulfide-linked receptor aggregates. *J. Biol. Chem.* 269, 22304–22309.
11. Cleveland, J.L. & Ihle, J.N. (1995). Contenders in FasL/TNF death signalling. *Cell* 81, 479–482.
12. Baker, S.J. & Reddy, E.P. (1996). Transducers of life and death: TNF receptor superfamily and associated proteins. *Oncogene* 12, 1–9.
13. Bajzer, Z., Myers, A.C. & Vuk-Pavlovic, S. (1989). Binding internalization and intracellular processing. *J. Biol. Chem.* 264, 13623–13631.
14. Engelmann, H., Novick, D. & Wallach, D. (1990). Two tumor necrosis factor-binding proteins purified from human urine. *J. Biol. Chem.* 265, 1531–1536.
15. Boldin, M.P., *et al*., & Wallach, D. (1995). Self-association of the 'death domains' of the p55 tumor necrosis factor (TNF) receptor and Fas/APO1 prompts signalling for TNF and Fas/APO1 effects. *J. Biol. Chem*. 270, 387–391.
16. Vuk-Pavlovic, S. & Kovach, J.S. (1989). Recycling of tumor necrosis factor-alpha-receptor in MCF-7 cells. *FASEB J*. 3, 2633–2640.
17. Lee, B. & Richards, F.M. (1971). The interpretation of protein structure: estimation of static accessibility. *J. Mol. Biol*. 55, 379–400.
18. Janin, J., Miller, S. & Chothia, C. (1988). Surface, subunit interfaces and interior of oligomeric proteins. *J. Mol. Biol*. 204, 155–164.
19. Janin, J. & Chothia, C. (1990). The structure of protein-protein recognition sites. *J. Biol. Chem*. 265, 16027–16030.
20. Finkelstein, J. & Janin, J. (1989). The price of lost freedom: entropy of bimolecular complex formation. *Protein Engineering* 3,1–3.
21. Rodseth, L.E., *et al*., & Sprang, S.R. (1994). Two crystal forms of the extracellular domain of type I tumor necrosis factor. *J. Mol. Biol.* 239, 332–335.
22. Otwinowski, Z. (1993). Oscillation Data Reduction Program. In *Proceedings of the CCP4 Study weekend: Data Collection and Processing*. (Sawyer, L., Isaacs, N. & Bailey, S., eds), pp. 56–62, Daresbury Laboratory, Warrington, U.K.
23. Collaborative Computing Project No. 4 (1994). The CCP4 Suite: programs for protein crystallography. *Acta Cryst. D* 50, 760–763.
24. Navaza, J. (1994). AMoRe: an Automated Package for Molecular Replacement. *Acta Cryst. A* 50, 157–163.
25. Brünger, A.T. (1990). X-PLOR (Version 2.1) Manual, Yale University, New Haven, USA.
26. Jones, T.A., Zou, J.-Y., Cowan, S.W. & Kjeldgaard, M. (1991). Improved methods for building protein models in electron density maps and the location of errors in these models. *Acta Cryst. A* 47, 110–119.
27. Read, R.J. (1986). Improved Fourier coefficients for maps using phases from partial structures with errors. *Acta Cryst. A* 42, 140–149.
28. Engh, R.A. & Huber, R. (1991). Accurate bond and angle parameters for X-ray protein structure refinement. *Acta Cryst. A* 47, 392–400.
29. Laskowski, R.A., MacArthur, M.W., Moss, D.S. & Thornton, J.M. (1993). PROCHECK: a program to check the stereochemical quality of protein structures. *J. Appl. Cryst.* 26, 548–558.
30. Bernstein, F.C., *et al*., & Tasumi, M. (1977). The protein databank: A computer-based archival file for macromolecular structure. *J. Mol. Biol.* 112, 535–542.
31. Merritt, E.A. & Murphy, M.E.P. (1994). Raster 3D version 2.O: A program for photorealistic graphics. *Acta Cryst. D* 50, 869–873.
32. Evans, S.V. (1993). SETOR: Hardware lighted three-dimensional solid model representations of macromolecules. *J. Mol. Graphics* 11, 134–138.
33. Lawrence, M.C. & Colman, P.M. (1993). Shape complementarity at protein/protein interfaces. *J. Mol. Biol.* 234, 946–950.